

## Molecular Dynamics Simulations of Surfactant Self-Organization at a Solid–Liquid Interface

Goundla Srinivas,<sup>\*,†,‡</sup> Steven O. Nielsen,<sup>†</sup> Preston B. Moore,<sup>§</sup> and Michael L. Klein<sup>†,‡</sup>

*Contribution from the Center for Molecular Modeling and the Department of Chemistry, University of Pennsylvania, Philadelphia, Pennsylvania 19104, The Laboratory for Research on the Structure of Matter, University of Pennsylvania, Philadelphia, Pennsylvania 19104-6202, and Department of Chemistry and Biochemistry, University of the Sciences in Philadelphia, Philadelphia, Pennsylvania 19104*

Received July 19, 2005; E-mail: srini@cmm.upenn.edu

**Abstract:** Self-organization of aqueous surfactants at a planar graphite-like surface is studied by means of coarse-grain molecular dynamics simulations. The nonionic surfactant, *n*-alkyl poly(ethylene oxide), and water are both represented by coarse-grain models while an implicit representation is used for the graphite surface. The observed morphology of the aggregated surfactants depends on the alkyl chain length. Surfactants with a short chain form a monolayer on the graphite surface with a thickness roughly equal to that of the alkane tail. On the other hand, longer-tail surfactants form continuous hemicylinders on the surface with diameter  $\sim 5.0 \pm 0.5$  nm, in good agreement with experimental AFM data.

### Introduction

Amphiphilic molecules tend to aggregate; however, their self-assembly at an interface can be different from that in the bulk solution.<sup>1–4</sup> Amphiphilic self-assembly in bulk solution results in a variety of distinct morphologies—bilayer and multilamellar vesicles, spherical and cylindrical (wormlike) micelles, and bicontinuous phases.<sup>1,5–7</sup> Recent experimental studies have revealed that many of the aggregate geometries seen in bulk solution can also be formed at the solid–liquid interface.<sup>8–12</sup> Nevertheless, the structure and shape of these aggregates exhibit different characteristics. The aggregation scenario at the solid–liquid interface differs from its bulk counterpart in many ways.<sup>1,2</sup> Interactions between surfactant solution and the solid surface

play a key role in this case. For example, graphite, a hydrophobic planar substrate, exerts two major influences on the adsorbing amphiphile geometry, namely (i) a specific interaction due to epitaxy of the alkyl chain with the graphite crystal and (ii) a nonspecific hydrophobic interaction between water and graphite which drives a minimization of the graphite–water interfacial area.

Adsorption of various amphiphiles on graphite as well as silica and mica (both hydrophobic and hydrophilic) has been studied extensively by different experimental techniques including adsorption isotherms,<sup>13</sup> surface force apparatus (SFA),<sup>14</sup> ellipsometry,<sup>15</sup> fluorescence decay,<sup>16–18</sup> neutron scattering,<sup>19–22</sup> and atomic force microscopy (AFM).<sup>8–12,23,24</sup> In the case of surfactants with alkyl tails, hydrophobic substrates such as graphite interact primarily with surfactant tail groups through van der Waals interactions. Non-hydrophobic surfaces do not show such behavior. In addition, it has been suggested that epitaxy is responsible for surfactant tail groups and alkane chains

<sup>†</sup> Center for Molecular Modeling and the Department of Chemistry, University of Pennsylvania.

<sup>‡</sup> The Laboratory for Research on the Structure of Matter, University of Pennsylvania.

<sup>§</sup> Department of Chemistry and Biochemistry, University of the Sciences in Philadelphia.

- (1) Israelachvili, J. N. *Intermolecular and Surface Forces*, 2nd ed.; Academic Press: London, 1992; pp 341–385.
- (2) Richard, C.; Balvoine, F.; Schultz, P.; Ebbesen, T. W.; Mioskowski, C. *Science*, **2003**, *300*, 775.
- (3) Manne, S.; Gaub, H. E. *Science* **1995**, *270*, 1482.
- (4) O'Connell, M. J.; Bachilo, S. M.; Huffman, C. B.; Moore, V. C.; Strano, M. S.; Haroz, E. H.; Rialon, K. L.; Boul, P. J.; Noon, W. H.; Kittrell, C.; Ma, J.; Hauge, R. H.; Weisman, R. B.; Smalley, R. E. *Science* **2002**, *297*, 593.
- (5) Rabe J. P.; Buchholz, S. *Science* **1991**, *253*, 424.
- (6) Helfrich, W. *J. Phys.: Condens. Matter* **1994**, *6*, A79.
- (7) Patrick, H. N.; Warr, G. G.; Manne, S.; Aksay, I. A. *Langmuir* **1997**, *13*, 4349.
- (8) Grant, L. M.; Tiberg, F.; Ducker, W. A. *J. Phys. Chem. B* **1998**, *102*, 4288.
- (9) Ducker, W. A.; Wanless, E. J. *Langmuir* **1999**, *15*, 160. Wanless, E. J.; Ducker, W. A. *Langmuir* **1997**, *13*, 1463.
- (10) Ducker, W. A.; Grant, L. M. *J. Phys. Chem. B* **1996**, *100*, 11507.
- (11) Manne, S.; Cleveland, J. P.; Gaub, H. E.; Stucky, G. D.; Hansma, P. K. *Langmuir* **1994**, *10*, 4409.
- (12) Jaschke, M.; Butt, H.-J.; Gaub, H. E.; Manne, S. *Langmuir* **1997**, *13*, 1381.

- (13) Fuerstenau, D. W. *J. Phys. Chem.* **1956**, *60*, 981–985.
- (14) Pashley, R. M.; Israelechvili, J. N. *Colloids Surf.* **1981**, *2*, 169. Pashley, R. M.; McGuiggan, P. M.; Horn R. G.; Ninham, B. W. *J. Colloid Interface Sci.* **1988**, *126*, 569.
- (15) Tilberg, F.; Jonsson, B.; Tang, J.; Lindmann, B. *Langmuir* **1994**, *10*, 2294.
- (16) Levitz, P.; El Meri, A.; Keravis, D.; Van Damme, H. *J. Colloid Interface Sci.* **1984**, *99*, 484.
- (17) Levitz, P.; Van Damme, H.; Keravis, D. *J. Phys. Chem.* **1984**, *88*, 2228–2235.
- (18) Levitz, P.; Van Damme, H. *J. Phys. Chem.* **1986**, *90*, 1302.
- (19) McDermott, D. C.; McCamey, J.; Thomas, R. K.; Rennie, A. R. *J. Colloid Interface Sci.* **1994**, *162*, 304.
- (20) Lee, E. M.; Thomas, R. K.; Cummins, P. G.; Staples, E. J.; Penfold, J.; Rennie, A. R. *Chem. Phys. Lett.* **1989**, *162*, 196.
- (21) McDermott, D. C.; Lu, J. R.; Lee, E. M.; Thomas, R. K.; Rennie, A. R. *Langmuir* **1992**, *8*, 1204.
- (22) Bohmer, M. R.; Koopal, L. K.; Janssen, R.; Lee, E. L.; Thomas, R. K.; Rennie, A. R. *Langmuir* **1992**, *8*, 2228.
- (23) Binnig, G.; Quate, C. F.; Gerber, Ch. *Phys. Rev. Lett.* **1986**, *56*, 930.
- (24) Wanless, E. J.; Ducker, W. A. *J. Phys. Chem.* **1996**, *100*, 3207–3214.

adsorbing parallel to a graphite symmetry axis, because the positions of the carbon atoms in the alkane chain closely match those of the graphite surface.<sup>11,25</sup> Nevertheless, similar surfactant aggregates at the same relative orientation on the cleavage plane of MoS<sub>2</sub> have been observed by Manne et al.<sup>3</sup> Furthermore, alkanes and aliphatic alcohols both form striped structures.<sup>2,25,26</sup> Hence, the common mechanism is speculated to be a crystalline anisotropy in van der Waals interactions rather than a specific correspondence between adsorbate and substrate atoms.<sup>3</sup>

Experimental studies of interfacial aggregation include zwitterionic surfactants on graphite, mica, gold, and silica. Manne et al.<sup>3</sup> showed that *n*-alkyl trimethylammonium bromide (CTAB) forms hemispherical micelles on graphite with a diameter of  $\sim 4.7 \pm 0.3$  nm, which was followed by a series of studies supporting their observation.<sup>6–9</sup> Nonionic surfactants have been found to adsorb strongly on graphite. Adsorption increases with increasing concentration up to the critical micelle concentration (cmc),<sup>27,28</sup> after which it remains fairly constant. Patrick et al.<sup>7</sup> studied the self-assembly structures of nonionic surfactants at graphite–liquid interfaces by varying the headgroup size. They have concluded that C12E3 (E represents an ethyleneglycol unit), which is geometrically capable of only forming bilayers as a bulk lyotropic phase, forms monolayers perpendicular to the graphite surface. On the other hand, C12E5, C12E8, and C12E10 which are capable of forming cylindrical micelles in solution, are found to form hemicylinders at the graphite–liquid interface. Later Ducker and co-workers<sup>10</sup> carried out systematic AFM studies of the self-organization of ethylene oxide surfactants by varying the alkane chain length on graphite as well as on hydrophobic and hydrophilic silica. This study allowed them to examine the influence of specific epitaxial binding of the alkyl chain.

The basic understanding from all of these studies is that the initial adsorption step for all amphiphilic molecules is a templated adsorption of the aliphatic chain along one of the graphite symmetry axes up to coverage by a horizontal monolayer. The striped phase thus formed orients subsequent adsorption, which occurs through hydrophobic association. Two-step adsorption isotherms of surfactants on graphite support this mechanism.<sup>28</sup>

Despite such extensive experimental studies, computational studies in this regard are scarce. An obvious choice to gain insights into the mechanism behind the experimental observations is to carry out computer simulations based on fully atomistic models. However, the time- and length scales for amphiphilic adsorption on a surface from the bulk solution are too long to be conveniently studied by such simulations.<sup>29–31</sup> The long time and length scales of such self-assembly phenomena put it beyond the reach of atomistic simulations. Balasubramanian et al.<sup>29</sup> studied adsorption on surfaces using an extremely detailed representation. Klein et al.<sup>30</sup> studied the interaction of

the CTAB surfactant with graphite by using a united atom model. Starting from a preassembled monolayer of CTAB at the graphite–water interface, they could show that the monolayer gradually reorganizes into hemicylinders. However, their study was restricted by a relatively small system size and short simulation time. Here, we adopt an intermediate coarse-grain simulation approach that can allow the study of such macroscopic self-assembly phenomena while still being computationally viable. Recent studies have shown that simulations based on coarse-grain models can successfully bridge the gap between specific atomistic simulations and generic stochastic modeling. For example, Smit et al.<sup>32</sup> observed the spontaneous self-assembly of surfactants into micelles for the first time by using such models. Lipowsky et al.,<sup>33</sup> Klein et al.,<sup>34–37</sup> and Marrink et al.<sup>38–41</sup> developed robust coarse grain models for biological systems. Schick and co-workers<sup>42</sup> successfully studied membrane fusion using coarse-grain models. These studies demonstrated the success of coarse-grain models in studying a variety of macroscopic phenomena, such as biomembrane self-assembly,<sup>34,36,37</sup> membrane<sup>42</sup> and vesicle fusion,<sup>40,41</sup> and ion translocation across a lipid bilayer.<sup>43</sup> Recently, we have developed a coarse grain model for diblock copolymers<sup>44</sup> and showed that they spontaneously self-assemble into various morphologies including bilayers, as well as both spherical and wormlike micelles depending on the hydrophilic content.<sup>45</sup> Accordingly, in this study we model both the surfactants and solvent (water) using a coarse grain (CG) approach, while an implicit representation is used for an immobile graphite surface. Even in atomistic simulations an implicit surface is commonly used.<sup>30,46</sup>

## Methods

In the present study we utilize a CG model for the nonionic surfactant, alkylpoly(ethylene oxide) (C<sub>*m*</sub>E<sub>*n*</sub>). In the CG representation we group three consecutive backbone atoms along with their hydrogen atoms into a single CG site. As noted in previous studies,<sup>34–36,47</sup> grouping three linear –CH<sub>2</sub>– entities into a single unit preserves the basic structural information reasonably well. The hydrophilic part

- (25) Yeo, Y. H.; Yackaboski, K.; McGonigal, G. C.; Thompson, D. J. *J. Vac. Sci. Technol.* **1992**, *A10*, 600–602.  
 (26) Groszek, A. J. *Proc. R. Soc. London, Ser. A* **1970**, *314*, 473–498.  
 (27) Findenegg, G. H.; Pasucha, B.; Strunk, H. *Colloids Surf.* **1989**, *37*, 223–233.  
 (28) Aston, J. R.; Furlong, D. N.; Grieser, F.; Scales, P. J.; Warr, G. J. In *Adsorption at the Gas/Solid and Liquid–Solid Interface*; Rouquerol, J., Sing K. S. W., Eds.; Elsevier: New York, 1982; pp 97–102.  
 (29) Krishnan, M.; Balasubramanian, S. *Phys. Chem. Chem. Phys.* **2005**, *7*, 2044.  
 (30) Bandyopadhyay, S.; Shelley, J. C.; Tarek, M.; Moore, P. B.; Klein, M. L. *J. Phys. Chem. B* **1998**, *102*, 6318.  
 (31) Werder, T.; Walther, T. H.; Jaffe, R. L.; Halicioglu, T.; Koumoutsakos, P. *J. Phys. Chem. B* **2003**, *107*, 1345 and references therein.

- (32) Smit, B.; Hilbers, P. A. J.; Esselink, K.; Rupert, L. A. M.; Van Os, N. M.; Schlijper, A. G. *J. Phys. Chem.* **1991**, *95*, 6361. Kranenburg, M.; Venturoli, M.; Smit, B. *J. Phys. Chem. B* **2003**, *107*, 11491. Venturoli, M.; Smit, B. *Phys. Chem. Commun.* **1999**, *10*.  
 (33) Goetz, R.; Gompper, G.; Lipowsky, R. *Phys. Rev. Lett.* **1999**, *82*, 221. Goetz, R.; Lipowsky, R. *J. Chem. Phys.* **1998**, *108*, 7397.  
 (34) Shelley, J. C.; Shelley, M.; Reeder, R.; Bandyopadhyay, S.; Klein, M. L. *J. Phys. Chem. B* **2001**, *105*, 4464. Shelley, J. C.; Shelley, M. Y.; Reeder, R. C.; Bandyopadhyay, S.; Moore, P. B.; Klein, M. L. *J. Phys. Chem. B* **2001**, *105*, 9785.  
 (35) Lopez, C. F.; Nielsen, S. O.; Moore, P. B.; Klein, M. L. *Proc. Natl. Acad. Sci. U.S.A.* **2004**, *101*, 4431.  
 (36) Nielsen, S. O.; Klein, M. L. In *Bridging Time Scales: Molecular Simulations for the Next Decade*; Nielaba, P., Mareschal, M., Ciccotti, G., Eds.; Springer: New York, 2002.  
 (37) Nielsen, S. O.; Lopez, C. F.; Moore, P. B.; Shelley, J. C.; Klein, M. L. *J. Phys. Chem. B* **2003**, *107*, 13911.  
 (38) Marrink, S. J.; Tieleman, D. P. *J. Am. Chem. Soc.* **2001**, *123*, 383. Marrink, S. J.; Mark, A. E. *J. Am. Chem. Soc.* **2003**, *125*, 144.  
 (39) Marrink, S. J.; Tieleman, D. P. *Biophys. J.* **2002**, *83*, 2386. Marrink, S. J.; Tieleman, D. P.; Mark, A. E. *J. Phys. Chem. B* **2000**, *104*, 12 165.  
 (40) Marrink, S. J.; Mark, A. E. *J. Am. Chem. Soc.* **2003**, *125*, 11144.  
 (41) de Vries, A. H.; Mark, A. E.; Marrink, S. J. *J. Am. Chem. Soc.* **2004**, *126*, 4488.  
 (42) Muller, M.; Kastov, K.; Schick, M. *J. Polym. Sci., Part B: Polym. Phys.* **2003**, *41*, 1441.  
 (43) Srinivas, G.; Lopez, C. F.; Klein, M. L. *J. Phys. Chem. B* **2004**, *108*, 4231.  
 (44) Srinivas, G.; Discher, D. E.; Klein, M. L. *Nat. Mater.* **2004**, *3*, 638; Srinivas, G.; Shelley, J. C.; Nielsen, S. O.; Discher, D. E.; Klein, M. L. *J. Phys. Chem. B* **2004**, *108*, 8153.  
 (45) Srinivas, G.; Discher, D. E.; Klein, M. L. *Nano Lett.* Published online October 18, <http://dx.doi.org/10.1021/nl051515x>.  
 (46) Lee, H. S.; Rossky, P. J. *J. Chem. Phys.* **1992**, *100*, 3334.  
 (47) Fukunaga, H.; Takimoto, J.; Doi, M. *J. Chem. Phys.* **2002**, *116*, 8183.

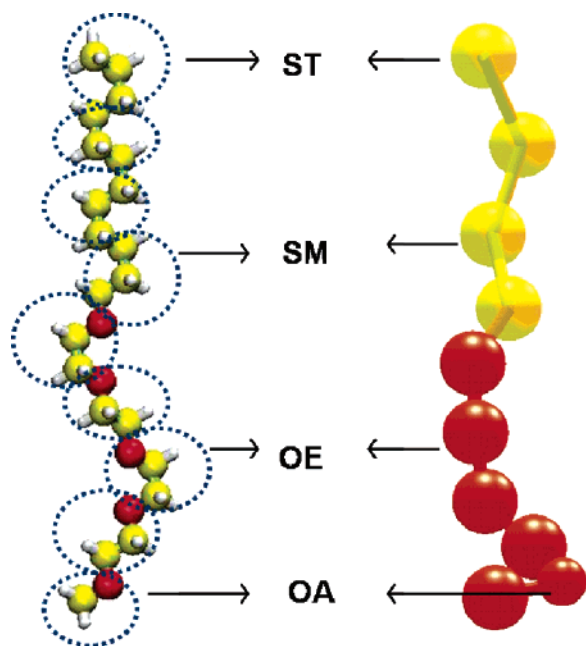


**Figure 1.** Coarse-grain mapping of an all-atom (AA) C12E5 surfactant molecule. The hydrophobic (CH<sub>2</sub>–CH<sub>2</sub>–CH<sub>2</sub>) and hydrophilic (CH<sub>2</sub>–CH<sub>2</sub>–O) monomer units are represented by coarse-grain units SM and OE, respectively. End groups, namely CH<sub>2</sub>–OH and CH<sub>2</sub>–CH<sub>2</sub>–CH<sub>3</sub>, are represented by OA and ST, respectively. Color for the AA scheme: oxygen - red, carbon - yellow, and hydrogen - white.

consists of ethylene oxide repeating units. The monomer unit –CH<sub>2</sub>–CH<sub>2</sub>–O– is grouped as a CG repeating unit and is represented by EO. In earlier studies, Klein et al.<sup>34</sup> developed a CG model for dimyristoylphosphatidylcholine (DMPC) lipids, which include hydrocarbon tails. Later they presented<sup>47</sup> a systematic method to coarse-grain alkane chains with any number of atoms. In the present study we use a similar method to determine the CG parameters for the alkyl part. In a previous study we developed the CG parameters for PEO–PEE diblock copolymers.<sup>43</sup> Hence, we have adopted the EO parameters from that work. The intermolecular interactions between EO and hydrophobic units (SM and ST, see Figure 1) are obtained by matching the CG simulation radial distribution functions with that obtained from all-atom simulations. Details of the coarse-grain procedure for all of these units including water (which is represented as a loose grouping of three real water molecules) can be found in our previous studies.<sup>34,35,44</sup> Nevertheless, we mention a few salient details here.

The CG polymer chain is constructed by using the center of mass position of each monomer in the corresponding all atom (AA) surfactant. Consecutive sites are bonded through a harmonic potential of the form,  $U_{\text{bond}}(r_{ij}) = (k_b/2)(r_{ij} - r_o)^2$  where the equilibrium bond distance is denoted by  $r_o$  and  $k_b$  is the bond force constant. The bond angle between three consecutive units is governed by a cosine angle potential,<sup>33</sup>  $U_{\text{bend}}(\theta_{ijk}) = k_\theta[(\theta_{ijk} - \theta_o)^2]$ , where  $\theta_{ijk}$  is the bond angle formed by sites  $i$ ,  $j$ , and  $k$  and  $\theta_o$  represents the equilibrium bond angle. Table 1 of the Supporting Information summarizes the bond distance and bond angle parameters needed for the present simulation. Wherever we have encountered the need for new parameters, we obtained them by comparing the corresponding target observable obtained from all atom simulations as before.<sup>33,34,44</sup>

In the present study we deal with two different surfactants, namely, penta(oxyethylene)-*n*-dodecyl ether (C12E5) and tri(oxyethylene)-*n*-decyl ether (C10E3). Prior to adsorption studies we have calculated various static and dynamic properties of these surfactants in bulk solution to test the robustness of the present model and presented them in the Supporting Information.

In the CG representation, the interacting sites are larger than their atomistic counterparts, resulting in much smoother potentials. The

nonbonded interactions among hydrophobic sites are modeled with Lennard-Jones potentials of the form,  $U(r_{ij}) = (27/4)\epsilon[(\sigma/r_{ij})^p - (\sigma/r_{ij})^q]$ ,  $\epsilon$  and  $\sigma$  correspond to the well-depth and van der Waals diameter of the corresponding species, respectively. We use  $p = 9$  and  $q = 6$  in this case. To determine the parameters  $\epsilon$  and  $\sigma$  we have chosen experimental bulk density and surface tension as target observables (taken from the literature<sup>47</sup>). Both  $\epsilon$  and  $\sigma$  are adjusted until the simulations satisfactorily reproduce experimental bulk density and surface tension, respectively. More details in this regard can be found elsewhere.<sup>43</sup> For the self-interaction among water (W) sites we use  $p = 6$  and  $q = 3$  in the L-J potential. We developed tabulated potentials for poly(ethylene glycol) in our earlier study.<sup>44</sup> The interacting potential parameters among and between all the CG units are presented in Table 2 of the Supporting Information.

Having parametrized the surfactants and water we turn our attention to graphite. Typically atomistic simulations involving a graphite–liquid interface use an implicit representation of graphite where the liquid particles interact with the surface through an external field.<sup>30,48–51</sup> We have developed a CG model for graphite in this spirit.<sup>52</sup> Briefly, the atomistic field experienced by each of the liquid atoms comprising a CG unit, along with the direct interactions between these atoms, is converted into an effective field between the center of mass of the atoms and the surface. This is accomplished by forming the probability distribution,  $P_i$ , from each atomistic potential  $U_i$  ( $P_i = \exp(-\beta U_i)$ ) multiplying them all together to get the joint distribution,  $P_{\text{joint}} = \prod_i P_i$ , and then computing the marginal distribution of the center of mass. Details on our implicit representation of graphite can be found in the Supporting Information.

**Simulation Details.** Surfactant molecules (C10E3 and C12E5) are constructed using the CG parameters mentioned above. Due to the CG representation, each surfactant has 7 (C10E3) or 10 (C12E5) CG units (including the end groups). The simulation system is constructed in a box with a basic unit containing 5 fully hydrated surfactants with 180 CG water sites. Although it is common to use a 10 fs time step in CG simulations, we employ a relatively smaller 3 fs time step in this work because of the implicit presence of the surface. The surfactants are initially placed randomly in water. This system is then allowed to relax and equilibrate at 303 K. We then replicated the simulation cell in the  $x$ -,  $y$ -, and  $z$ -directions  $4 \times 4 \times 5$  times, respectively, to generate a larger system. After delicate adjustments to remove overlapping water molecules, the final resulting system contains 400 surfactants and 14 400 CG water sites, corresponding to more than 43 000 real water molecules. As before, the simulation system is allowed to relax and equilibrate at 303 K for  $1.8 \times 10^5$  time steps. As mentioned in earlier studies,<sup>34,52</sup> the CG approach involves smoother potentials, which essentially results in time scales that are 2 orders of magnitude larger than all atom simulation times. All the times reported in this article are in terms of the number of time steps employed in the simulations.

The solid–liquid interfaces are present in the simulation cell, a distance  $d$  ( $=12$  nm) apart. Given the field between a liquid particle at height  $z > 0$  above a solid surface at  $z = 0$ ,  $U(z)$ , the particles in our setup experience a field  $(U(d/2 + z) + U(d/2 - z))$  between surfaces at  $z = -d/2$  and  $z = d/2$ . In practice three-dimensional periodic boundary conditions are used by taking the unit cell to have a height in the  $z$ -direction larger than  $d$ , so that the solid surfaces are separated on one side with liquid and on the other side with enough vacuum to form a buffer zone through which all the interaction potentials decay essentially to zero.  $U(z)$  decays to zero by 2.4 nm, much shorter than the graphite–graphite interseparation (12 nm).

(48) Nielsen, S. O.; Lopez, C. F.; Srinivas, G.; Klein, M. L. *J. Chem. Phys.* **2003**, *119*, 7043.

(49) *Physical Properties of Polymers Handbook*; Mark, J. E., Ed.; American Institute of Physics: New York, 1996.

(50) Shelley, J. C.; Patey, G. N. *J. Mol. Phys.* **1996**, *88*, 385.

(51) Hentschke, R.; Schurmann, B. L.; Rabe, P. *J. Chem. Phys.* **1992**, *96*, 6213.

(52) Nielsen, S. O.; Srinivas, G.; Lopez, C. F.; Klein, M. L. *Phys. Rev. Lett.* **2005**, *94*, 228301.

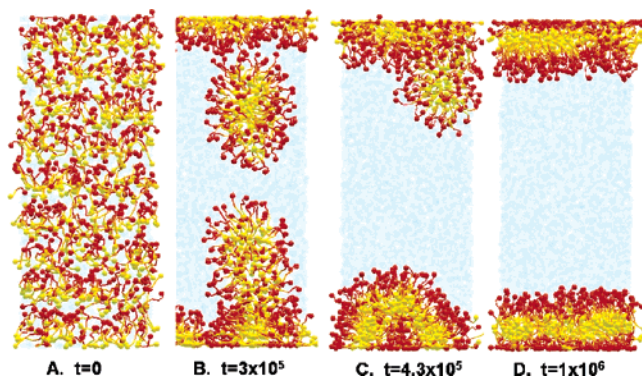


**Figure 2.** Adsorption of C10E3 surfactants onto graphite surfaces from bulk solution as observed in coarse-grain molecular dynamics simulations. Graphite surfaces are placed one above and one below the water + surfactant slab. Water is shown in light blue. Surfactant end groups are shown by ball representation, while the rest of the surfactant is represented by a stick representation. (A) Initial configuration, (B) and (C) self-assembled surfactants getting adsorbed onto graphite surfaces by the feeding mechanism, and (D) monolayer formation after self-organization.

## Results and Discussion

We studied the self-assembly and self-organization of both C10E3 and C12E5 surfactants. We describe the results for each system separately. However, prior to self-assembly, to study both the robustness of the present CG model and the surfactant self-assembly in bulk water we carried out simulations of water–surfactant binary mixtures with varying mole fractions. Transport properties obtained from CG simulations are found to be in good agreement with the experimental findings.<sup>53</sup> Similar results are obtained by using C10E3 surfactants (details can be found in the Supporting Information).

**C10E3 Adsorption on Graphite.** Snapshots of the C10E3 simulation with the graphite surface are presented in Figure 2. From the initial random configuration, surfactants begin coating the graphite surface (Figure 2A). Simultaneously, they start self-assembling in the bulk water away from the surface. The initial coating is fast because the surface is uncoated, and the adsorption rate decreases gradually as the surface becomes coated. This is expected, since the surface becomes increasingly unavailable for adsorption with time. However, the self-assembly in bulk solution becomes predominant once the graphite surface is fully coated. Structural analysis shows that during the initial coating stages the alkyl tails lay horizontal on the graphite surface. At this stage the surfactants in bulk water feel less attraction toward the surface because their interaction with the surface is screened. As a result, the adsorption rate decreases drastically. A snapshot after  $0.3 \times 10^5$  time steps is shown in Figure 2B. As shown, at this stage the surfactants remaining in bulk water self-assemble and form a spherical micelle. This also reveals that these surfactants are capable of forming micelles in bulk water by spontaneous self-assembly. In the process of random motion, this micelle diffuses toward one of the graphite surfaces.

A completely different adsorption method is observed once the micelle reaches the graphite vicinity. The surfactant headgroups near the surface interact with those of the surfactants already adsorbed on the graphite.<sup>54,55</sup> At this point, we find that the micelle starts “feeding” the graphite surface (Figure 2B).

The feeding mechanism transfers aqueous surfactant aggregates to the semi-coated graphite surface. As the extent of feeding increases, the thickness of the monolayer also increases, indicating that the surfactants start changing their orientation from near parallel to perpendicular on the graphite surface. “Feeding” continues until the entire micelle is adsorbed onto the graphite surface. The C10E3 adsorption thus leads to an aggregate with the shape of a near perfect monolayer on the graphite surface. This aggregate continues to reorganize itself until it forms a monolayer coating the graphite surface as shown in Figure 2D. However, the complete adsorption of the micelle onto the graphite surface indicates that the surfactant concentration might not be sufficient to cover the entire graphite surface utilized in the present simulations. We will come to this point during the discussion of C12E5 adsorption.

**C12E5 Adsorption on Graphite.** The adsorption mechanism of C12E5 is similar to that of C10E3 during the initial stages. The initial fast coating followed by the slow adsorption rate is observed in this case as well. However, the micelle formation in bulk is predominant in this case. We observe the formation of two separated micelles in the center of the simulation cell (which is the farthest distance from either of the graphite surfaces). We find that, despite the occasional interactions, these micelles do not fuse into a single micelle. This reveals that the micelles are saturated in terms of surfactant concentration. As before, when a micelle reaches the vicinity of a graphite surface, it gets dragged toward the surface. Once again the micelle adsorbs onto the graphite surface by a “feeding” mechanism, as described in the case of C10E3. The surfactant concentration on the surface increases. At this point, the other micelle moves toward the opposite surface and starts feeding (see Figure 3). By a similar mechanism the micelle gets adsorbed onto the other surface.

Once the adsorption process is completed, reorganization starts. The self-organization on a graphite surface in this case results in the formation of hemicylinders as shown in Figure 3F. A different view of this structure shows that these hemicylindrical structures extend in the direction parallel to the graphite surface and they are indeed hemicylinders rather than hemispheres (Figure 4). Such hemicylinder formation has been observed in experimental studies and is a focus of active debate. This is the first such simulation study to observe hemicylindrical formation on a solid substrate. The lateral spacing between hemicylinders is calculated as  $5.0 \pm 0.5$  nm, which agrees well with the experimental predictions.<sup>3</sup>

To study whether such a structural feature is just a coincidence, we have constructed two different additional simulation systems (i) with a system size 4 times the size mentioned above (1600 surfactants) and (ii) another system with lower surfactant concentration (see the Supporting Information). In both the cases simulations yielded results similar to those above, revealing that the hemicylindrical aggregates observed in our simulations are indeed not influenced by the starting configuration of the

(53) Lopez, C. F.; Moore, P. B.; Shelley, J. C.; Shelley, M. Y.; Klein, M. L.; *Comput. Phys. Commun.* **2002**, *147*, 1.

(54) Feitosa, E.; Brown, W.; Vasilescu, M.; Swanson-Vethamuthu, M.; *Macromolecules* **1996**, *29* (21), 6837.

(55) In principle, when the micelle reaches a partially coated surface, the polyethylene headgroups repel each other due to electrostatic interactions. We speculate that the strong attractive interaction between the graphite surface and carbon atoms of surfactant dominates. As a result micelles gradually get adsorbed onto the graphite surfaces.

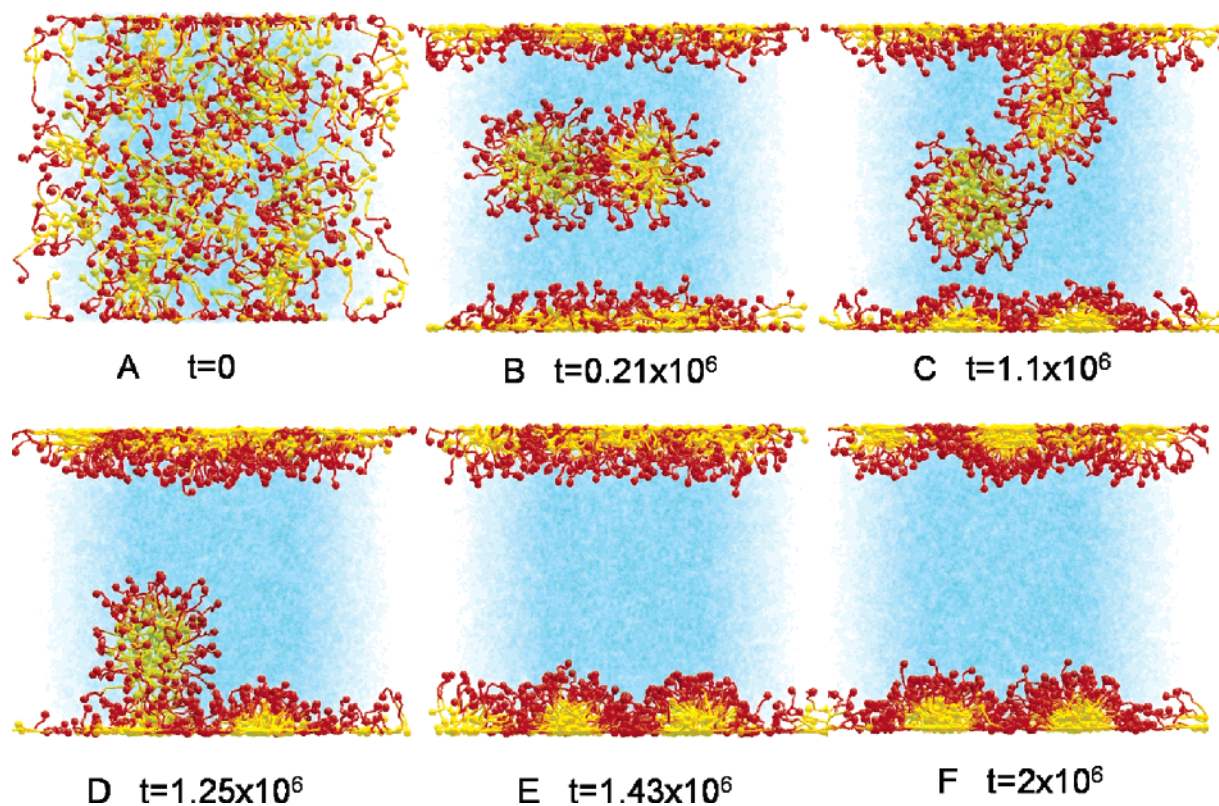


**Figure 3.** Snapshots of C12E5 surfactant adsorption onto hydrophobic surfaces as observed in CG simulations. Color and other details are identical to those in Figure 2.

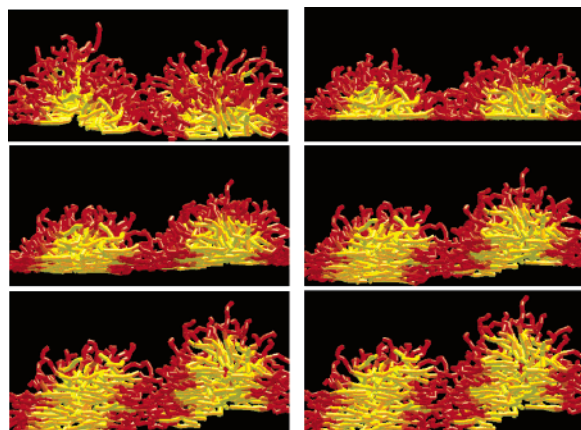


**Figure 4.** Hemicylinders formed by C12E5 surfactant adsorption onto a graphite surface are shown in different orientations. Snapshots are tilted (relative to each other) away from the graphite surface. Water is not shown for clarity. An additional figure is presented in the Supporting Information.

simulation system. Hence, we conclude that the hemicylinder formation on graphite is a common feature for this class of surfactants.

The surfactant adsorption mechanism onto a graphite surface is studied in more detail. Figure 5 shows the number of C12E5 surfactants adsorbed onto the graphite surfaces as a function of time. Simulations reveal that the initial rapid adsorption is followed by a slow reorganization for a long time. After  $1.3 \times 10^6$  time steps, a sudden jump in the adsorption kinetics is observed, a time when one of the micelles reaches the surface vicinity and starts “feeding”. The time points corresponding to micelle adsorption by the “feeding mechanism” are marked as A, B, and C. This is observed for both the surfaces and is highlighted by a circle in Figure 5. Once the micelle is

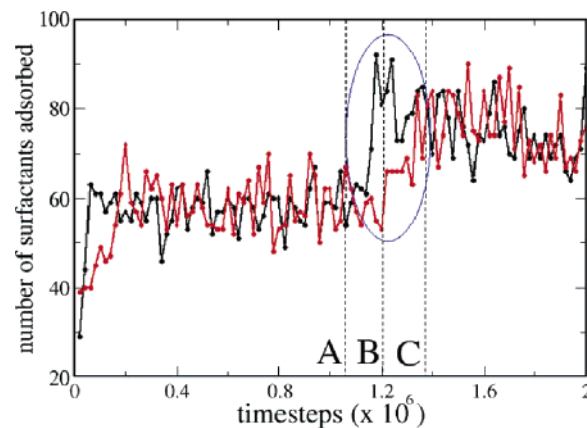


**Figure 5.** Number of surfactants adsorbed onto each of the graphite surfaces is shown separately (black and red) as a function of simulation time. Increase in adsorption at later stages is due to micelle “feeding” and is highlighted by a circle. The crucial time steps for micelle adsorption are marked by A, B, and C.

completely adsorbed onto the surface, self-organization begins as explained above, leading to the final configuration as shown in Figures 3F and 4. A similar but relatively faster feeding mechanism is observed in the case of C10E3.

In Figure 6 relevant thermodynamic quantities for three different components (namely the hydrophobic and hydrophilic parts of the surfactant and water) are plotted as a function of simulation time. As shown in Figure 6I, the enthalpies of both hydrophilic and hydrophobic blocks of the surfactant significantly decrease during the adsorption process. Nevertheless, the hydrophobic block shows a relatively larger decrease. This reveals that the hydrophobic interaction with the surface might be relatively more important in driving the adsorption process.

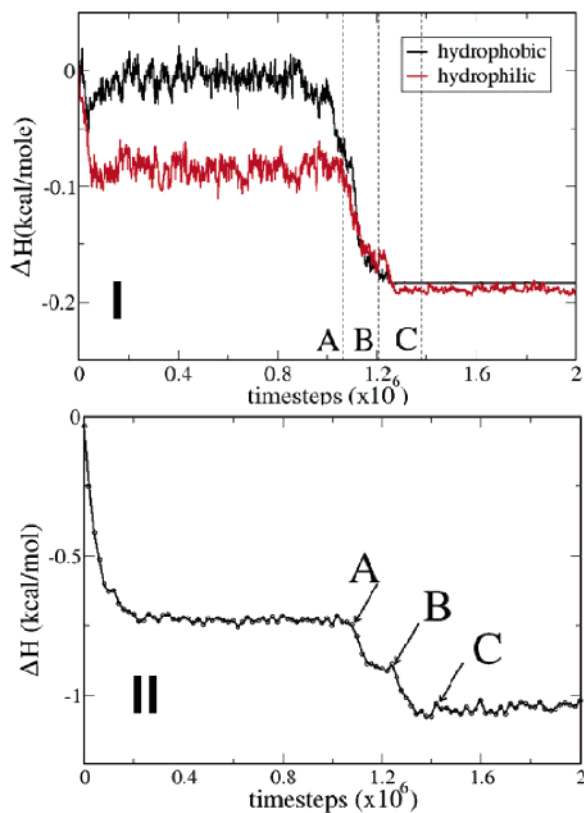


**Figure 6.** Enthalpy variation during the surfactant adsorption onto graphite surfaces is shown as a function of simulation time. (I) Both hydrophilic and hydrophobic blocks show similar decreases in enthalpy. (II) Results for water are shown. In all the figures A, B, and C represent the corresponding time steps shown in Figure 5.

Interestingly, water contributes to a great extent toward lowering enthalpy as shown in Figure 6II. This can be interpreted in a straightforward manner. The initially self-assembled surfactant micelle gets adsorbed onto the graphite surface by dislodging the water molecules in the vicinity of the graphite surface, thereby reducing the water contact with the hydrophobic surface. After the initial decrease in enthalpy (as shown in Figure 6II) during the micelle adsorption, two major dips in the enthalpy curve are observed (marked by A and B in the figure). Each dip corresponds to a surfactant micelle adsorption on graphite surface). On the other hand, during the self-organization process no significant variation in enthalpy is observed.

## Conclusions

We have studied the adsorption of nonionic surfactants onto a graphite surface by means of coarse-grain molecular dynamics

simulations. The CG approach allowed us to probe macroscopic phenomena such as self-assembly, adsorption, and self-organization of the surfactants at reasonable length and time scales with affordable computational effort. Prior to the adsorption studies we studied the dynamics of individual surfactants in bulk water as a function of mole fraction. This allowed us to test the performance of the present CG model for nonionic surfactant systems. We found that both C10E3 and C12E5 show similar adsorption kinetics. In both cases a rapid adsorption rate is followed by slower adsorption as the surfaces saturate with surfactants. This mechanism transfers entire surfactant aggregates from the aqueous phase to the solid–liquid interface. Once graphite reaches a semi-coated stage, micelle formation is observed in bulk water. The “feeding” mechanism, by which the aggregates that have been self-assembled in bulk water adsorb onto the semi-coated graphite surface, is found to be effective in both cases. Once the adsorption is completed, the surfactants start reorganizing. The self-organization in the case of C10E3 results in a near perfect monolayer, while hemicylinder formation parallel to the graphite surface is observed in the case of C12E5. The hemicylinder diameter is found to be  $5.0 \pm 0.5$  nm, in good agreement with the experimental predictions.<sup>3</sup> Additionally, insights into the adsorption mechanism are provided by the enthalpy studies.

Since the adsorption on a graphite surface has been explored successfully, as a next step it would be interesting to extend the present model to study the adsorption of similar (and other) surfactants on materials such as carbon nanotubes.<sup>2,4</sup> Such studies will not only test the present generic model but might also provide novel insights into the mechanism of separation of carbon nanotubes from bundles and ropes. Indeed, studies in this direction are currently under active investigation.

**Acknowledgment.** We thank the NIH and the NSF for their support and Carlos Lopez for his interest.

**Supporting Information Available:** (i) Coarse-grain parametrization details for all the components; (ii) competitive adsorption of mixed alkanes on graphite surface; (iii) initial results for a larger system to examine the system size influence and (iv) C12E5 adsorption at lower concentration. This information is available free of charge via the Internet at <http://pubs.acs.org>.

JA054846K